Environmental Science: Atmospheres

ROYAL SOCIETY OF CHEMISTRY

COMMUNICATION

View Article Online
View Journal

Cite this: DOI: 10.1039/d5ea00049a

Received 24th April 2025
Accepted 17th June 2025

DOI: 10.1039/d5ea00049a

rsc.li/esatmospheres

Dependence of black carbon restructuring on the volatility of biomass burning organic aerosol coatings at the wildland–urban interface†

Christian A. Escritt, Katrina L. Betz, Micah R. Miles and Elijah G. Schnitzler *

Biomass burning organic aerosol (BBOA) and black carbon (BC) play significant roles in climate, *via* their interactions with light and clouds, as well as public health. BC in the urban atmosphere, largely emitted by diesel vehicles, is initially highly branched and fractal, but it can be restructured upon coating. Urban BC aggregates can be exposed to the components of BBOA when wildfire plumes cross the wildland–urban interface (WUI), which may partition to coat the BC. Here, we investigate the effects of laboratory-generated BBOA from pine on BC from an inverted diffusion burner. Initially 200 nm BC aggregates were selected using a differential mobility analyzer (DMA) and exposed to different volatility fractions of BBOA. These fractions were prepared by evaporative aging in the laboratory, which mimics evaporative aging with transport in the atmosphere, to give fresh, moderately aged, and most aged BBOA. The resulting mobility diameters with and without removal of the coating were determined using a second DMA. We find that an exceedingly small coating volume of fresh (*i.e.*, higher volatility) BBOA causes complete restructuring while a significantly higher coating volume of most aged (*i.e.*, lower volatility) BBOA is necessary for this same extent of restructuring. Our results highlight the importance of evaporative age of BBOA as wildfire plumes are transported across the WUI into urban environments.

Environmental significance

Wildland fires are a significant source of primary organic aerosol, called biomass burning organic aerosol (BBOA). When this material crosses the wildland–urban interface (WUI), it can interact with urban black carbon (BC), uncoated aggregates with fractal, highly branched structures, emitted largely from diesel engines. Specifically, it can partition onto BC, resulting in restructuring due to surface tension and capillary forces. Here, we show in saturator–condenser experiments that fresh BBOA from sources close to the WUI is more effective by volume at restructuring BC than evaporatively aged BBOA from sources far from the WUI. The resulting morphologies dictate how the particles will interact with radiation and water vapor, interactions that govern their direct and indirect effects on climate, respectively.

1. Introduction

Black carbon (BC) aggregates affect air quality as well as the radiative balance of the atmosphere, through interactions with light and clouds.[1] BC aggregates are composed of spherical primary particles of elemental carbon arranged in highly branched, fractal morphologies,[2,3] which dictate how the particles interact with light.[4,5] BC aggregates may also accumulate coatings that alter these interactions through lensing effects.[6–8] These coatings may induce restructuring of the BC aggregates, resulting in more compact, closely-packed morphologies.[9] Coatings that have been observed to induce BC restructuring in laboratory experiments include water,[10,11] sulphuric acid,[12,13] and secondary organic aerosol (SOA) from a wide range of gaseous precursors: *e.g.*, biogenic isoprene and α-pinene;[14–17] anthropogenic benzene,[18] toluene,[18,19] ethylbenzene,[18] and *m*- and *p*-xylene;[18,20,21] and co-emitted combustion byproducts.[22,23] Water is important also for its ability to plasticize solid organic coatings or deliquesce solid inorganic coatings, such that the liquified coatings can go on to induce restructuring.[24,25] For some coatings, like water, the mechanism of restructuring is evaporation of the coating;[10,26] for others, the mechanism of restructuring is a combination of condensation and evaporation.[27–29] Several models of restructuring have been developed to represent the forces (*e.g.*, capillary and surface tension) acting on the primary particles in coated BC aggregates.[20,30–32] For initially monodisperse BC, the combination of restructuring and coating has been observed to result in significant absorption enhancement.[13,19,33] In the atmosphere, coated BC aggregates occur across a wide range of morphologies, differing the amount of BC (*i.e.*, few or many primary particles), the amount of coating (*i.e.*, thinly or thickly coated), the compactness of the BC (*i.e.*, branched or closely packed), and the distribution of the coating on the BC (*i.e.*, centric or

Department of Chemistry, Oklahoma State University, Stillwater, OK 74078, USA. E-mail: elijah.schnitzler@okstate.edu

† Electronic supplementary information (ESI) available. See DOI: https://doi.org/10.1039/d5ea00049a

acentric).[34–36] This wide range of morphologies further complicates the physical and optical properties of BC.[37,38]

BC is an important component of the urban atmosphere, where it is largely emitted from diesel vehicles.[39,40] The initial morphology of BC from diesel engines has been investigated and shown to be highly branched.[41–43] Branched aggregates produced from diesel engines in the laboratory have been shown to be compacted upon coating.[44,45] Urban BC has also been shown to be coated and compacted in the field.[46–48] Nascent, monodisperse BC introduced into an outdoor semi-permeable chamber, where it was exposed to gaseous species in two urban atmospheres, also was coated and compacted.[33] The occurrence of BC in the urban atmosphere that is initially largely bare contrasts with BC in wildfire plumes that is initially internally mixed with organic aerosol, called biomass burning organic aerosol (BBOA),[49] which influences the physical and optical properties of co-emitted BC across a range of mass fractions, as described above.[50–53] Wildfires have been shown to influence the organic composition of suspended particles and deposited films in the urban environment;[54,55] for example, wildfires increase the concentration of polycyclic aromatic hydrocarbons (PAHs) in the urban atmosphere.[55] Several PAHs have been shown to restructure BC aggregates in the laboratory as sub-cooled liquids.[56] Consequently, when wildfire plumes cross the wildland–urban interface (WUI),[57–59] urban BC is exposed to the components of BBOA, which may alter the morphology of the BC aggregates. Furthermore, BBOA is a complex mixture of organic species with wide ranges of physical and chemical properties,[60–62] which may influence its interactions with urban BC.

Here, we focus on the following hypotheses: first, components of BBOA will partition to form coatings on nascent, highly branched BC aggregates and, in turn, induce restructuring to give a more compact, closely-packed morphology; and, second, the effects of BBOA on BC morphology will depend on the physical properties of this complex mixture, which change during transport in the atmosphere. BC was generated using an inverted diffusion flame, and aggregates with an initial mobility diameter of 200 nm were selected using a differential mobility analyzer (DMA). BBOA was generated by thermal degradation of pine wood in a tube furnace, and filter-collected samples were conditioned by evaporative aging. Monodisperse BC was exposed to conditioned BBOA in a saturator–condenser apparatus, and the resulting mobility diameters with and without thermal denuding were monitored using a second DMA coupled to a condensation particle counter (CPC). Our results and their atmospheric implications are discussed below.

2. Materials and methods

2.1. Generation of BC

BC was generated using a miniature inverted soot generator (Argonaut) with ethylene as the fuel.[63,64] The flowrates of ethylene (Airgas, Ultra High Purity) and air (Airgas, Ultra Zero Grade) were set to 0.1 and 10 L min^{-1}, respectively, using mass flow controllers (Sensirion, SFM5500 Series). The flowrates were verified using a bubble-based calibrator (Sensidyne, Gilibrator 2). As shown in Fig. 1c, a small fraction of the output of the soot generator, at a flowrate of 0.3 L min^{-1}, was directed through a denuder with a length of 60 cm, consisting of stainless-steel mesh packed in granular activated carbon (Sigma-Aldrich, SBHL1410). This sample was then sent through two diffusion dryers, the first with a length of 43 cm and the second (TSI, 3062) with a length of 44 cm, both packed with indicating silica gel desiccant (Parker, DRP-14-10B). The conditioned aerosol was then directed to an electrostatic

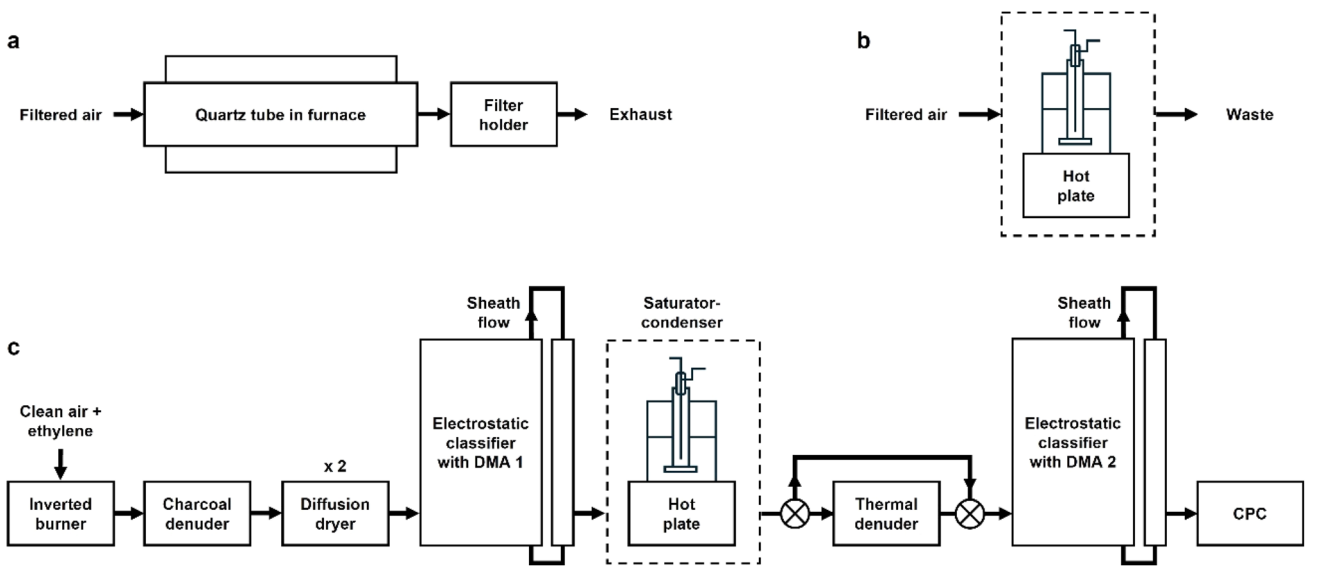

Fig. 1 Schematic of experimental setups for the (a) generation of BBOA, (b) evaporative aging of BBOA, and (c) the generation, coating, and characterization of BC aggregates. The saturator–condenser apparatus consists of a glass bubbler in a sand bath on the hot plate, and the filter-collected and conditioned BBOA is placed at the base of the bubbler while the hot plate temperature is ramped during coating. DMA: differential mobility analyzer; CPC: condensation particle counter.

classifier (TSI, 3082), equipped with a 0.0457 cm nozzle upstream of the inertial impactor, a soft X-ray advanced aerosol neutralizer (TSI, 3088), and a long DMA (TSI, 3081). The sample and sheath flowrates of the DMA were 0.3 and 3 L min^{-1}, respectively. The DMA voltage was set to select particles with an electrical mobility diameter of 200 nm.

2.2. Generation and characterization of BBOA

BBOA was generated by thermal degradation, without flaming, of pine wood in a tube furnace (Across International, STF1200), described previously.[65,66] This method is an alternative to combustion chambers, used for highly realistic burns in some studies,[67–69] and has been used extensively since it allows precise control of temperature and flow velocity.[70–72] A rectangular chip of pine wood was placed at the center of the 5 cm diameter quartz tube that is housed in the furnace. The average mass of pine was about 3.5 g. Air (Airgas, Ultra Zero Grade) was directed through the quartz tube at a flowrate of 1.5 L min^{-1}. The tube furnace was programmed to increase in temperature from 25 °C to 400 °C in 15 min. At 350 °C, the generation of BBOA began, a polycarbonate filter holder (Pall, 1119) was connected to the inlet, and BBOA was collected onto a pre-weighed 47 mm fiber filter (Pall, Emfab) for about 1 min (see Fig. 1a). The filter-collected BBOA was then weighed to determine the mass of BBOA collected on the filter paper and stored in a freezer (Fisher, Isotemp) at −15 °C for later use in the coating experiments.

In this study, BBOA was generated for the purpose of coating BC; before the coating experiments, three categories of BBOA were prepared, differing in conditioning, *i.e.*, evaporative aging, and the resulting volatility distribution. In the first category, called fresh, BBOA collected on a filter was used without further conditioning. In the second category, called moderately aged, BBOA on the same filter after the previous experiment was subjected to evaporative conditioning, passing 3 L min^{-1} of clean, dry air from a zero-air generator (Aadco, 747-30) over the filter in a 250 mL glass bubbler, heated to 60 °C, for 48 h (see Fig. 1b). In the third category, called most aged, BBOA on the same filter after the previous two experiments was subjected to further evaporative conditioning, passing 3 L min^{-1} of clear, dry air over the filter, heated to 120 °C, for 48 h. The heating was performed on a hot plate using a sand bath, in which the bubbler was immersed about 3 cm from the base. Mass losses with each step of conditioning were determined gravimetrically using an analytical balance. Three replicates of this sequence of conditioning were performed.

BBOA was characterized in terms of absorptivity using UV-vis spectroscopy of bulk solutions of BBOA extracted into methanol. Spectra were measured for three filter-collected samples, conditioned respectively to give fresh, moderately aged, and most aged BBOA. Each filter sample was placed in a vial containing 10 mL of methanol (Fisher, >99.8%), and the vial was placed on a roller mixer for 15 min at 60 rpm. The pre-weighed filter paper was removed, dried, and weighed to determine the mass concentration of BBOA in each solution. An aliquot of each solution was used in a 1 cm quartz cuvette for spectroscopic measurements *via* a modular fiber-optic-based spectrometer, which consists of a balanced deuterium-halogen light source (Ocean Optics, DH-2000-BAL), a cuvette holder with lenses (Thorlabs, CVH100), and a grating-based spectrometer (Ocean Insight, Flame-T-UV-vis). The measured absorbances along with the known mass concentrations of BBOA in each sample were used to calculate mass absorption coefficients of the bulk solutions, MAC_{bulk}, using the following equation:

$$MAC_{bulk} = \frac{A_{10}^{solution} \ln(10)}{l_{solution} C_{mass}} \quad (1)$$

Here, $A_{10}^{solution}$ is the absorbance of the solution at a given wavelength, $l_{solution}$ is the pathlength through the cuvette (*i.e.*, 1 cm), and C_{mass} is the BBOA mass concentration in the solution. The MAC_{bulk} values were not corrected for Mie resonances, necessary to be applied to suspended particles.[73–75]

2.3. Characterization of particles upon coating

BC was coated by passing it over the BBOA collected on filters, which was conditioned as described above. The size-selected BC was directed through a clean 250 mL glass bubbler with the selected category of filter-collected BBOA at the bottom (see Fig. 1c). The flowrate through the bubbler was 0.3 L min^{-1}. Like above, heating was performed using a sand bath. Here, the temperature was increased incrementally, up to 142 °C for the most aged, least volatile category of BBOA. Downstream of the bubbler, which serves as the saturator, the sample was returned to room temperature before being directed through one of two paths, alternately. In the first path, the sample was passed through a 1.8 m thermal denuder, constructed from 1/4″ copper tubing, as described previously.[66,76] The temperature of the thermal denuder was set to 200 °C. The particles were then directed to a second DMA, which was equipped the same as the first and operated at the same flowrates, and a CPC (TSI, 3750). The sample flowrate of the CPC is 1 L min^{-1}, so the difference of 0.7 L min^{-1} was sampled from the laboratory through a particle filter. In the second path, the sample bypassed the thermal denuder. In a control experiment, BBOA was also used to coat spherical monodisperse polystyrene latex particles (Polysciences, 64 000 Series), and sheath flowrates of 3, 4.5, and 6 L min^{-1} on the second DMA gave the same mobility diameters for coated particles (see Fig. S1†), suggesting that evaporation between the condenser and DMA was insignificant.

3. Results and discussion

3.1. Evaporative aging of BBOA

The filter-collected BBOA was conditioned by preparatory evaporation, flowing clean, dry air through the filters, to produce BBOA differing in evaporative aging and, in turn, volatility and absorptivity. Here, pine was used as the source of BBOA, as it is common in regions with increasing instances of wildfires (*e.g.*, the northwestern US[77]) and has previously been used in laboratory studies of other properties and processes of BBOA,[62,78,79] facilitating integration of our results into a broader

understanding of BBOA from this source. The mass of fresh BBOA collected on the filters was 110 ± 10 mg. After the first step of conditioning, to produce what is here called moderately aged BBOA, 0.61 ± 0.02 of the fresh BBOA mass remained. After the second step of conditioning, to produce the most aged BBOA, 0.33 ± 0.04 of the fresh BBOA mass remained. The fraction remaining for the most aged BBOA closely matches the largest increment used in recent studies of the effects of evaporative aging on the viscosity and absorptivity of BBOA from hardwood pellets, where this fraction was called PO_3 to denote the volume was reduced by a factor of three from that of the initial pyrolysis oil.[60,80] This preparatory evaporation mimics in the laboratory the partitioning of BBOA components downwind of a fire,[61,81] and is similar to approaches used previously to simulate evaporative aging.[66,82] Increased evaporative aging is known to result in decreased BBOA volatility, with corresponding changes in composition measured using high-resolution mass spectrometry coupled to liquid chromatography.[60,80] The MAC of the remaining BBOA also increased with evaporative aging, as shown in Fig. 2 for solutions in methanol. All but 0.9 mg of each sample was soluble in methanol on average (*i.e.*, over 98% extraction efficiency). At 365 nm, MAC was 0.26, 0.57, and 0.73 $m^2\ g^{-1}$ for fresh, moderately aged, and most aged BBOA. The mass of the most aged BBOA is precisely one third that of the fresh, and the MAC at 365 nm of the fresh is just slightly greater than one third that of the most aged. At 405 nm, MAC was 0.07, 0.18, and 0.32 $m^2\ g^{-1}$ for fresh, moderately aged, and most aged BBOA. The significant increase in MAC with evaporative aging indicates that the most volatile components of BBOA, which partition out of the particle phase, are much less absorptive than the components that remain in the particle phase. This observation is consistent with previous observations for BBOA produced from other fuels, *i.e.*, hardwood pellets and eastern red cedar,[60,66] supporting the use of the material produced here as representative BBOA. The variable absorptivity of BBOA will result in different effects on the optical properties of BC aggregates upon coating.[52,53,83]

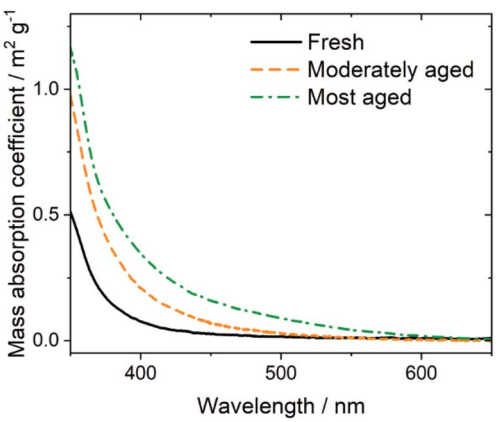

Fig. 2 Mass absorption coefficients for differently conditioned BBOA fractions in methanol solutions.

3.2. Restructuring of BC upon coating with BBOA

The conditioned BBOA was used to coat BC aggregates, which were first selected by size at a mobility diameter of 200 nm from the polydisperse size distribution characteristic of the burner and combustion conditions.[63] The miniature inverted soot generator produced a stable size distribution of BC, as shown in Fig. S2.† We note that the particles selected at 200 nm occur to the right, *i.e.*, higher mobility diameter, than the geometric mean diameter. This choice of initial diameter ensures that singly charged particles are the most abundant, as opposed to doubly or multiply charged particles with larger dimensions. These sized particles are also representative of the average-size BC particles from urban and wildfire sources, as well as those found in pyrocumulonimbus clouds.[84] Monodisperse, size-selected particles were monitored using the second DMA in combination with the CPC, stepping through voltages and measuring the resulting number concentration. Representative size spectra are shown in Fig. S3.† Changes in morphology upon coating and restructuring were determined by monitoring the monodisperse particles. Each size spectrum was fit to a lognormal peak. The center of the peak was used to quantify the change in mobility diameter, and the geometric standard deviation was used to ensure the particles remained monodisperse.[85,86]

A representative coating experiment with the moderately aged BBOA is shown in Fig. 3b, in terms of the mobility diameters of both denuded (*i.e.*, coated–uncoated) and non-denuded (*i.e.*, coated) particles as a function of the saturator temperature. The experiment can be divided into three stages. In the first stage, between 20 and 50 °C, the denuded and non-denuded particles exhibited the same morphology as the initial size-selected aggregates indicating no restructuring is caused by thermal denuding. For these saturator temperatures and this BBOA volatility fraction (*i.e.*, moderately aged), the vapor pressures of the components were too low to result in partitioning onto the BC. During the second stage, between 50 and 70 °C, the mobility diameters of both classes of particles began decreasing. The denuded particles decreased in diameter throughout this stage, until they approached a plateau for the final, fully restructured aggregates, resulting in a sigmoidal curve. The non-denuded particles (*i.e.*, with coating intact) also decreased in diameter initially during this stage, demonstrating that condensation rather than evaporation is driving most of the restructuring in BBOA-coated BC. This is not the case for all coatings; for example, water is known to cause significant restructuring only upon evaporation, a distinction that may be attributed to whether a coating effectively wets the BC surface or not.[10] This observation also demonstrates that the BBOA coating was a liquid. Fresh BBOA has previously been shown to be liquid.[62,66] While evaporative aging is known to increase the viscosity of BBOA,[60,87] attributed to greater mass contributions of larger, more polarizable molecules (*i.e.*, with stronger van der Waals interactions), here it was still sufficiently low-viscosity to restructure the aggregates on the experimental timescale, *i.e.*, the residence time between the saturator and the second DMA. The non-denuded particles followed the trend of the denuded

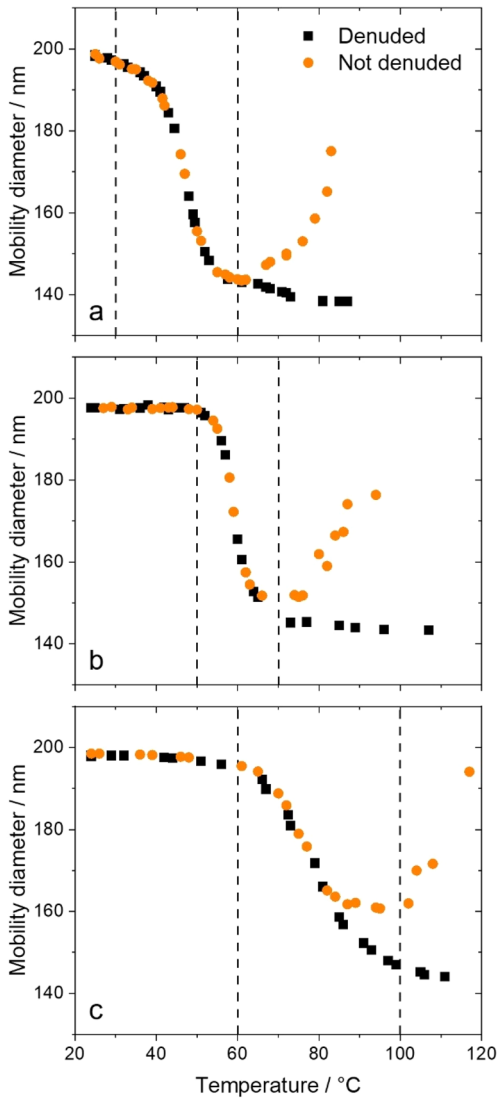

Fig. 3 Representative experiments with (a) fresh, (b) moderately aged, and (c) most aged BBOA, showing evolution of the mobility diameter of particles with and without thermal denuding as a function of increasing saturator temperature, which drives partitioning of BBOA components onto the BC aggregates. Dashed lines represent the three distinct regions of the experiments: little to no restructuring, significant restructuring, and near-complete restructuring of the BC core, respectively.

particles until a saturator temperature of about 65 °C, at which point they diverged, reaching a minimum and beginning to grow. During the third stage of the experiment, between 70 and 110 °C, the mobility diameter of the denuded particles reached its plateau, *i.e.*, the aggregates could not restructure further, no matter how much coating material partitioned onto the BC. The mobility diameter of the non-denuded particles continued increasing, as more material was added to the coating, according to the temperature dependence of the vapor pressures of the BBOA components (*i.e.*, governed by the Clausius–Clapeyron equation).[88,89] The elevated saturator temperatures are not meant to represent atmospherically relevant temperatures but allow us to probe high volume growth factors with BBOA, much the same way that elevated precursor mixing ratios allow others to probe high volume growth factors with SOA.[18,19]

3.3. Dependence of BC restructuring on BBOA volatility

These three stages of evolution are also observed for BC aggregates coated with fresh and most aged BBOA, but the temperatures associated with the three stages are different. For fresh BBOA, the first stage occurs only at very low temperatures. Already at 30 °C, sufficient BBOA begins to partition to result in some restructuring (see Fig. 3a). Again, the trends for denuded and non-denuded particles overlap, indicating that the restructuring occurs during condensation rather than evaporation of the coating in the thermal denuder. For most aged BBOA, the temperature required for restructuring to begin is about 60 °C (see Fig. 3c). For fresh BBOA, the two series overlap for the duration of the second stage of restructuring. It is only when the BC cores are fully restructured, reaching the plateau at the final extent of restructuring, that the two series diverge (see Fig. 3a). In other words, very little coating is required to fully restructure the BC aggregates for fresh BBOA. For most aged BBOA, the two datasets diverge halfway through the second stage of evolution (see Fig. 3c), well before the aggregates are fully restructured, indicating that the coating required to induce complete restructuring is higher for this less volatile fraction of BBOA. During the third stage of the experiments, the exponential increase in mobility diameter of the fully restructured aggregates with coating intact is an indication that these particles were spherical. The fully restructured aggregates without coating are known to be not quite spherical, with mass-mobility exponents (see ESI†) of about 2.7–2.8 (*i.e.*, less than the value of 3 expected for spheres),[9,18,45] but in an approximation they are taken as spherical here, such that their volume may be estimated from their mobility diameter.

To estimate the volume of coating, we take the difference between the volume of the coated particles and volume of the restructured cores, with coating removed, both calculated according to their respective mobility diameters (see ESI†). This difference is shown in Fig. S4† for a representative experiment with the fresh BBOA, the same as depicted in Fig. 3a. The subtraction of volumes assumes spherical geometries, an approximation that is only reasonable after the BC cores approach their final diameter, during the third stage of the coating experiment, described above. Another constraint is that, at the initial saturator temperature, no BBOA partitioning onto BC occurs, so the coating volume is zero at 25 °C. Fitting an exponential function, meant to capture the temperature dependence of the vapor pressures of the BBOA components, to these first and third stages of the coating experiment, we obtain the curve shown in Fig. S4.† From this fit, coating volume at any temperature can be estimated by interpolation.

When the diameter growth factor of the restructured BC aggregates without coating is plotted as a function of the volume growth factor of the aggregates with coating intact (see ESI†), differences between the BBOA volatility fractions are further evident. As shown in Fig. 4, fresh BBOA (*i.e.*, without any evaporative conditioning before the coating experiment)

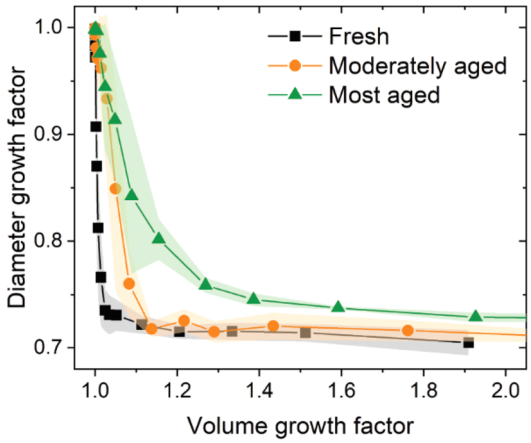

Fig. 4 Diameter growth factor of coated-denuded BC aggregates as a function of volume growth factor of coated particles for differently conditioned BBOA coatings. Experiments were performed in triplicate, and the shaded regions depict inter-experiment variance in terms of one standard deviation. The individual replicate experiments are shown in Fig. S5.†

induced significant restructuring at very low coating volumes. At a volume growth factor of 1.1 (*i.e.*, when the coating volume is 10% of the initial aggregate volume), the diameter growth factor was already approaching its final value of about 0.70. For moderately aged BBOA, the diameter growth factor at the same volume growth factor is about 0.75. In other words, at the same coating volume, this fraction is less effective at restructuring the BC aggregates than the fresh BBOA. For most aged BBOA, the same volume growth factor of 1.1 leads to a diameter growth factor of only 0.85, about halfway between the initially branched and fully restructured aggregates. To reach the plateau for completely restructured BC aggregates with most aged BBOA, the coating volume must approach 100% of the initial aggregates volume, ten times greater than for fresh BBOA.

How can these differences between the volatility fractions of BBOA in terms of their ability to induce restructuring of BC aggregates be rationalized? Based on their study of pure liquid coatings, Chen *et al.* proposed a single-parameter framework of soot aggregate restructuring.[30] The single parameter, χ, is expressed as follows:

$$\chi = \frac{l_K}{R_s}\frac{1}{\zeta} \quad (2)$$

where l_K is the Kelvin length, R_s is the radius of the spherical primary particles, and ζ is the reduced (*i.e.*, dimensionless) vapor supersaturation of the coating species. In our experiments, the conditions were carefully controlled to give the same initial aggregate morphology,[45] so the value of R_s is expected to be consistent between experiments. The Kelvin length varies with the surface tension of the coating species; however, this effect is smaller than the effect of volatility, through changes in ζ.[20,30] When χ is much less than unity, the coating partitions uniformly across the surface of the soot aggregates; when χ approaches unity, the coating partitions preferentially into the junctions between neighbouring primary particles, *i.e.*, constituent spherules of the aggregates.[30] By volume, coatings following this latter pathway are more effective at inducing restructuring of BC aggregates. As volatility increases, χ increases, as well. Consequently, pure high-vapor-pressure coatings (*e.g.*, triethylene glycol and tetradecane) caused aggregates to restructure to their final morphology already at mass growth factors of less than 1.1. In contrast, pure low-vapor-pressure coatings (*e.g.*, dioctyl sebacate and oleic acid) caused aggregates to restructure only partially at the same mass growth factors, a few percent opposed to the final diameter growth factor of 0.80 observed for the high-vapor-pressure coatings. Note the final extent of restructuring is highly dependent on the initial morphology of the soot aggregates, including the size and number of primary particles,[45] so it is not surprising that the final diameter growth factor in our experiments, about 0.70, is different than those reported in the earlier study with pure liquid coatings. More importantly, the relationship between coating volatility and its distribution on the BC aggregates allows us to rationalize our current results: fresh BBOA components on average have higher vapor pressures than evaporatively aged BBOA components, so they partition preferentially in the junctions between primary particles, inducing complete restructuring with little volume.

4. Atmospheric implications

Our results have broad implications on the interactions between BBOA from wildland fires and BC from urban sources at the WUI. Each volatility fraction of BBOA induced restructuring of BC aggregates upon partitioning, with the coating intact, demonstrating that compaction occurs without coating evaporation. This observation stands in contrast with restructuring induced by water, which requires evaporation,[10] and it is an important feature of the interactions between BBOA and BC, since many BBOA components, with lower volatilities, would not be expected to partition from the coated aggregates back into the gas phase. The restructuring induced by the most aged BBOA also demonstrates that even the most viscous volatility fraction acts as a liquid in the internally mixed particles.[24,56] Furthermore, the differences observed between the fresh, moderately aged, and most aged BBOA demonstrate that volatility largely governs the impact of BBOA coatings on BC aggregate morphology. Fresh BBOA, emitted from wildfires near the WUI, is most effective at restructuring BC aggregates; *i.e.*, coating volumes as little as 10% of the initial BC volume are sufficient to induce complete restructuring of BC aggregates to their final, most closely-packed morphology. As the evaporative age of BBOA increases, for emissions of wildfires at increasing distances from the WUI, the BBOA becomes less effective at inducing soot restructuring. For the most aged BBOA investigated here, 33% by mass of the initial BBOA, coating volumes about 100% of the initial BC volume (*i.e.*, doubling the total particle volume) are required to induce complete restructuring of BC aggregates to their final morphology. Not only is more coating required, less BBOA (*i.e.*, primary) material is available to partition upon dilution of the plume of wildfire emissions.[61,81] This also suggests that BC emitted from wildfires is likely to be promptly restructured as high concentrations of

fresh BBOA are co-emitted. This dependence on BBOA volatility can be rationalized in the context of the single-parameter framework of soot restructuring;[30] by volume, less fresh BBOA is required for complete restructuring because this material partitions preferentially into the junctions between neighbouring BC primary particles, whereas aged BBOA partitions more uniformly across the BC aggregate surface. This application of the single-parameter framework to complex mixtures of atmospherically relevant organic species, specifically those emitted from wildland fires, further emphasizes the utility of this framework.[30] Other processes, including irradiation and oxidative aging, may also influence the volatility of BBOA, so these may be considered in the future.[49,66] As wildfires continue to increase in frequency and severity in many regions,[77,90] wildfire plumes of BBOA are more likely to interact with urban BC at the WUI. The morphology of coated BC aggregates influences their interactions with solar and terrestrial radiation, water vapor, and the respiratory tract, so these volatility-dependent impacts on morphology will influence the effects of BC on human health through climate and air quality.

Data availability

Data for this article, including the figures in the main text and ESI,† are available on Zenodo at **https://doi.org/10.5281/zenodo.15277790**.

Conflicts of interest

There are no conflicts to declare.

Acknowledgements

The authors thank Ed Wright, Wes Cash, and Larry Vaughn for technical and fabrication support. They also thank Ogochukwu Enekwizu (Brookhaven National Laboratory) and Alexei Khalizov (New Jersey Institute of Technology) for helpful discussions on the single-parameter framework for restructuring and two anonymous reviewers for their helpful comments. This research was funded by the National Science Foundation through Grant AGS-2339449.

References

1 V. Ramanathan and G. Carmichael, Global and regional climate changes due to black carbon, *Nat. Geosci.*, 2008, **1**, 221–227.
2 T. A. Sipkens, A. Boies, J. C. Corbin, R. K. Chakrabarty, J. Olfert and S. N. Rogak, Overview of methods to characterize the mass, size, and morphology of soot, *J. Aerosol Sci.*, 2023, **173**, 106211.
3 L. Peng, Z. Li, G. Zhang, X. Bi, W. Hu, M. Tang, X. Wang, P. Peng and G. Sheng, A review of measurement techniques for aerosol effective density, *Sci. Total Environ.*, 2021, **778**, 146248.
4 M. Kahnert and F. Kanngießer, Modelling optical properties of atmospheric black carbon aerosols, *J. Quant. Spectrosc. Radiat. Transfer*, 2020, **244**, 106849.
5 G. A. Kelesidis, D. Neubauer, L.-S. Fan, U. Lohmann and S. E. Pratsinis, Enhanced Light Absorption and Radiative Forcing by Black Carbon Agglomerates, *Environ. Sci. Technol.*, 2022, **56**, 8610–8618.
6 G. Lefevre, J. Yon, M. Bouvier, F. Liu and A. Coppalle, Impact of Organic Coating on Soot Angular and Spectral Scattering Properties, *Environ. Sci. Technol.*, 2019, **53**, 6383–6391.
7 O. Enekwizu, D. Singh and A. Khalizov, Absorption and scattering of light by soot aggregates with uniform and pendular ring coatings, *J. Aerosol Sci.*, 2020, **147**, 105583.
8 J. Luo, Y. Zhang and Q. Zhang, A model study of aggregates composed of spherical soot monomers with an acentric carbon shell, *J. Quant. Spectrosc. Radiat. Transfer*, 2018, **205**, 184–195.
9 T. A. Sipkens and J. C. Corbin, Effective density and packing of compacted soot aggregates, *Carbon*, 2024, **226**, 119197.
10 X. Ma, C. D. Zangmeister, J. Gigault, G. W. Mulholland and M. R. Zachariah, Soot aggregate restructuring during water processing, *J. Aerosol Sci.*, 2013, **66**, 209–219.
11 E. F. Mikhailov and S. S. Vlasenko, Structure and optical properties of soot aerosol in a moist atmosphere: 1. Structural changes of soot particles in the process of condensation, *Izv., Atmos. Oceanic Phys.*, 2007, **43**, 181–194.
12 J. Pagels, A. F. Khalizov, P. H. McMurry and R. Y. Zhang, Processing of Soot by Controlled Sulphuric Acid and Water Condensation—Mass and Mobility Relationship, *Aerosol Sci. Technol.*, 2009, **43**, 629–640.
13 R. Zhang, A. F. Khalizov, J. Pagels, D. Zhang, H. Xue and P. H. McMurry, Variability in morphology, hygroscopicity, and optical properties of soot aerosols during atmospheric processing, *Proc. Natl. Acad. Sci. U. S. A.*, 2008, **105**, 10291–10296.
14 A. F. Khalizov, Y. Lin, C. Qiu, S. Guo, D. Collins and R. Zhang, Role of OH-Initiated Oxidation of Isoprene in Aging of Combustion Soot, *Environ. Sci. Technol.*, 2013, **47**, 2254–2263.
15 K. Li, L. Chen, K. Han, B. Lv, K. Bao, X. Wu, X. Gao and K. Cen, Smog chamber study on aging of combustion soot in isoprene/SO_2/NO_x system: changes of mass, size, effective density, morphology and mixing state, *Atmos. Res.*, 2017, **184**, 139–148.
16 H. Saathoff, K.-H. Naumann, M. Schnaiter, W. Schöck, O. Möhler, U. Schurath, E. Weingartner, M. Gysel and U. Baltensperger, Coating of soot and $(NH_4)_2SO_4$ particles by ozonolysis products of α-pinene, *J. Aerosol Sci.*, 2003, **34**, 1297–1321.
17 C. Yuan, Y. Ma, A. Khalizov, L. Wang, J. Zheng and R. Zhang, Impacts of α-pinene ozonolysis products on the morphology and optical properties of black carbon, *Atmos. Environ.*, 2024, **321**, 120337.
18 E. G. Schnitzler, A. Dutt, A. M. Charbonneau, J. S. Olfert and W. Jäger, Soot Aggregate Restructuring Due to Coatings of Secondary Organic Aerosol Derived from Aromatic Precursors, *Environ. Sci. Technol.*, 2014, **48**, 14309–14316.

19 C. Qiu, A. F. Khalizov and R. Zhang, Soot Aging from OH-Initiated Oxidation of Toluene, *Environ. Sci. Technol.*, 2012, **46**, 9464–9472.
20 E. G. Schnitzler, J. M. Gac and W. Jäger, Coating surface tension dependence of soot aggregate restructuring, *J. Aerosol Sci.*, 2017, **106**, 43–55.
21 S. Guo, M. Hu, Y. Lin, M. Gomez-Hernandez, M. L. Zamora, J. Peng, D. R. Collins and R. Zhang, OH-Initiated Oxidation of *m*-Xylene on Black Carbon Aging, *Environ. Sci. Technol.*, 2016, **50**, 8605–8612.
22 J. Leskinen, A. Hartikainen, S. Väätäinen, M. Ihalainen, A. Virkkula, A. Mesceriakovas, P. Tiitta, M. Miettinen, H. Lamberg, H. Czech, P. Yli-Pirilä, J. Tissari, G. Jakobi, R. Zimmermann and O. Sippula, Photochemical Aging Induces Changes in the Effective Densities, Morphologies, and Optical Properties of Combustion Aerosol Particles, *Environ. Sci. Technol.*, 2023, **57**, 5137–5148.
23 T. Tritscher, Z. Jurányi, M. Martin, R. Chirico, M. Gysel, M. F. Heringa, P. F. DeCarlo, B. Sierau, A. S. H. Prévôt, E. Weingartner and U. Baltensperger, Changes of hygroscopicity and morphology during ageing of diesel soot, *Environ. Res. Lett.*, 2011, **6**, 034026.
24 K. K. Leung, E. G. Schnitzler, W. Jäger and J. S. Olfert, Relative Humidity Dependence of Soot Aggregate Restructuring Induced by Secondary Organic Aerosol: Effects of Water on Coating Viscosity and Surface Tension, *Environ. Sci. Technol. Lett.*, 2017, **4**, 386–390.
25 A. C. Eriksson, C. Wittbom, P. Roldin, M. Sporre, E. Öström, P. Nilsson, J. Martinsson, J. Rissler, E. Z. Nordin, B. Svenningsson, J. Pagels and E. Swietlicki, Diesel soot aging in urban plumes within hours under cold dark and humid conditions, *Sci. Rep.*, 2017, **7**, 12364.
26 W. R. Heinson, P. Liu and R. K. Chakrabarty, Fractal scaling of coated soot aggregates, *Aerosol Sci. Technol.*, 2017, **51**, 12–19.
27 O. Y. Enekwizu, A. Hasani and A. F. Khalizov, Vapor Condensation and Coating Evaporation Are Both Responsible for Soot Aggregate Restructuring, *Environ. Sci. Technol.*, 2021, **55**, 8622–8630.
28 E. V. Ivanova, A. F. Khalizov and G. Y. Gor, Kinetic model for competitive condensation of vapor between concave and convex surfaces in a soot aggregate, *Aerosol Sci. Technol.*, 2020, **55**, 302–315.
29 J. C. Corbin, R. L. Modini and M. Gysel-Beer, Mechanisms of soot-aggregate restructuring and compaction, *Aerosol Sci. Technol.*, 2023, **57**, 89–111.
30 C. Chen, O. Y. Enekwizu, X. Fan, C. D. Dobrzanski, E. V. Ivanova, Y. Ma, G. Y. Gor and A. F. Khalizov, Single Parameter for Predicting the Morphology of Atmospheric Black Carbon, *Environ. Sci. Technol.*, 2018, **52**, 14169–14179.
31 P. Beeler, J. C. Corbin, T. A. Sipkens and L. Fierce, A Framework for Quantifying the Size and Fractal Dimension of Compacting Soot Particles, *Environ. Sci. Technol.*, 2025, **59**, 5994–6003.
32 H. Ishimoto, R. Kudo and K. Adachi, A shape model of internally mixed soot particles derived from artificial surface tension, *Atmos. Meas. Tech.*, 2019, **12**, 107–118.
33 J. Peng, M. Hu, S. Guo, Z. Du, J. Zheng, D. Shang, M. L. Zamora, L. Zeng, M. Shao, Y.-S. Wu, J. Zheng, Y. Wang, C. R. Glen, D. R. Collins, M. J. Molina and R. Zhang, Markedly enhanced absorption and direct radiative forcing of black carbon under polluted urban environments, *Proc. Natl. Acad. Sci. U. S. A.*, 2016, **113**, 4266–4271.
34 B. Romshoo, T. Müller, A. Ahlawat, A. Wiedensohler, M. V. Haneef, M. Imran, A. B. Warsi, A. K. Mandariya, G. Habib and M. L. Pöhlker, Significant contribution of fractal morphology to aerosol light absorption in polluted environments dominated by black carbon (BC), *npj Clim. Atmos. Sci.*, 2024, **7**, 1–10.
35 K. Hu, D. Liu, P. Tian, Y. Wu, Z. Deng, Y. Wu, D. Zhao, R. Li, J. Sheng, M. Huang, D. Ding, W. Li, Y. Wang and Y. Wu, Measurements of the Diversity of Shape and Mixing State for Ambient Black Carbon Particles, *Geophys. Res. Lett.*, 2021, **48**, e2021GL094522.
36 W. Li, N. Riemer, L. Xu, Y. Wang, K. Adachi, Z. Shi, D. Zhang, Z. Zheng and A. Laskin, Microphysical properties of atmospheric soot and organic particles: measurements, modeling, and impacts, *npj Clim. Atmos. Sci.*, 2024, **7**, 1–14.
37 L. Zeng, T. Tan, G. Zhao, Z. Du, S. Hu, D. Shang and M. Hu, Overestimation of black carbon light absorption due to mixing state heterogeneity, *npj Clim. Atmos. Sci.*, 2024, **7**, 1–8.
38 X.-F. Huang, Y. Peng, J. Wei, J. Peng, X.-Y. Lin, M.-X. Tang, Y. Cheng, Z. Men, T. Fang, J. Zhang, L.-Y. He, L.-M. Cao, C. Liu, C. Zhang, H. Mao, J. H. Seinfeld and Y. Wang, Microphysical complexity of black carbon particles restricts their warming potential, *One Earth*, 2024, **7**, 136–145.
39 S. Takahama, L. M. Russell, C. A. Shores, L. C. Marr, J. Zheng, M. Levy, R. Zhang, E. Castillo, J. G. Rodriguez-Ventura, P. J. E. Quintana, R. Subramanian, M. Zavala and L. T. Molina, Diesel vehicle and urban burning contributions to black carbon concentrations and size distributions in Tijuana, Mexico, during the Cal-Mex 2010 campaign, *Atmos. Environ.*, 2014, **88**, 341–352.
40 M. Zavala, L. T. Molina, T. I. Yacovitch, E. C. Fortner, J. R. Roscioli, C. Floerchinger, S. C. Herndon, C. E. Kolb, W. B. Knighton, V. H. Paramo, S. Zirath, J. A. Mejía and A. Jazcilevich, Emission factors of black carbon and co-pollutants from diesel vehicles in Mexico City, *Atmos. Chem. Phys.*, 2017, **17**, 15293–15305.
41 C. Han, S.-M. Li, P. Liu and P. Lee, Size Dependence of the Physical Characteristics of Particles Containing Refractory Black Carbon in Diesel Vehicle Exhaust, *Environ. Sci. Technol.*, 2019, **53**, 137–145.
42 Y. Pang, M. Chen, Y. Wang, X. Chen, X. Teng, S. Kong, Z. Zheng and W. Li, Morphology and Fractal Dimension of Size-Resolved Soot Particles Emitted From Combustion Sources, *J. Geophys. Res.: Atmos.*, 2023, **128**, e2022JD037711.
43 J. Olfert and S. Rogak, Universal relations between soot effective density and primary particle size for common combustion sources, *Aerosol Sci. Technol.*, 2019, **53**, 485–492.
44 D. Li, J. Wei, H. Chen, C. Wang and C. Wang, Study on the restructuring of soot particles from diesel engine exhaust

gas discharged into a simulated atmospheric environment, *Fuel*, 2023, **349**, 128679.
45 K. K. Leung, E. G. Schnitzler, R. Dastanpour, S. N. Rogak, W. Jäger and J. S. Olfert, Relationship between Coating-Induced Soot Aggregate Restructuring and Primary Particle Number, *Environ. Sci. Technol.*, 2017, **51**, 8376–8383.
46 A. K. Y. Lee, C.-L. Chen, J. Liu, D. J. Price, R. Betha, L. M. Russell, X. Zhang and C. D. Cappa, Formation of secondary organic aerosol coating on black carbon particles near vehicular emissions, *Atmos. Chem. Phys.*, 2017, **17**, 15055–15067.
47 Y. Wang, F. Liu, C. He, L. Bi, T. Cheng, Z. Wang, H. Zhang, X. Zhang, Z. Shi and W. Li, Fractal Dimensions and Mixing Structures of Soot Particles during Atmospheric Processing, *Environ. Sci. Technol. Lett.*, 2017, **4**, 487–493.
48 G. Zhao, M. Hu, W. Lin, Y. Kuang, J. Sun, L. Zeng and C. Zhao, Could We Achieve the On-Line Measurements of the Optical Fractal Dimensions of Black Carbon?, *Geophys. Res. Lett.*, 2025, **52**, e2024GL112332.
49 A. J. I. Sedlacek, E. R. Lewis, T. B. Onasch, P. Zuidema, J. Redemann, D. Jaffe and L. I. Kleinman, Using the Black Carbon Particle Mixing State to Characterize the Lifecycle of Biomass Burning Aerosols, *Environ. Sci. Technol.*, 2022, **56**, 14315–14325.
50 Z. Zhang, Y. Wang, X. Chen, L. Xu, Z. Zheng, J. Ching, S. Zhu, D. Liu and W. Li, Absorption enhancement and shielding effect of brown organic coating on black carbon aerosols, *npj Clim. Atmos. Sci.*, 2025, **8**, 1–9.
51 H. Chen, D. Hu, L. Wang, A. Mellouki and J. Chen, Modification in light absorption cross section of laboratory-generated black carbon-brown carbon particles upon surface reaction and hydration, *Atmos. Environ.*, 2015, **116**, 253–261.
52 X. Zhang, M. Mao, H. Chen, Y. Yin and S. Tang, Lensing Effect of Black Carbon With Brown Coatings: Dominant Microphysics and Parameterization, *J. Geophys. Res.: Atmos.*, 2021, **126**, e2020JD033549.
53 J. Luo, Y. Zhang, F. Wang and Q. Zhang, Effects of brown coatings on the absorption enhancement of black carbon: a numerical investigation, *Atmos. Chem. Phys.*, 2018, **18**, 16897–16914.
54 R. M. Healy, J. M. Wang, C.-H. Jeong, A. K. Y. Lee, M. D. Willis, E. Jaroudi, N. Zimmerman, N. Hilker, M. Murphy, S. Eckhardt, A. Stohl, J. P. D. Abbatt, J. C. Wenger and G. J. Evans, Light-absorbing properties of ambient black carbon and brown carbon from fossil fuel and biomass burning sources, *J. Geophys. Res.: Atmos.*, 2015, **120**, 6619–6633.
55 I. Chan, S. R. Schneider, A. Cheng and S. A. Styler, Wildfire Smoke Contributions to Polycyclic Aromatic Hydrocarbon Loadings in Western Canadian Urban Surface Grime, *Environ. Sci. Technol.*, 2025, **59**, 2745–2753.
56 C. Chen, X. Fan, T. Shaltout, C. Qiu, Y. Ma, A. Goldman and A. F. Khalizov, An unexpected restructuring of combustion soot aggregates by subnanometer coatings of polycyclic aromatic hydrocarbons, *Geophys. Res. Lett.*, 2016, **43**, 11080–11088.
57 Y. Guo, J. Wang, Y. Ge and C. Zhou, Global expansion of wildland-urban interface intensifies human exposure to wildfire risk in the 21st century, *Sci. Adv.*, 2024, **10**, eado9587.
58 W. Tang, L. K. Emmons, C. Wiedinmyer, D. B. Partha, Y. Huang, C. He, J. Zhang, K. C. Barsanti, B. Gaubert, D. S. Jo, J. Zhang, R. Buchholz, S. Tilmes, F. Vitt, C. Granier, H. M. Worden and P. F. Levelt, Disproportionately large impacts of wildland-urban interface fire emissions on global air quality and human health, *Sci. Adv.*, 2025, **11**, eadr2616.
59 J. M. Silberstein, L. E. Mael, C. R. Frischmon, E. S. Rieves, E. R. Coffey, T. Das, W. Dresser, A. C. Hatch, J. Nath, H. O. Pliszka, C. E. Reid, M. E. Vance, C. Wiedinmyer, J. A. De Gouw and M. P. Hannigan, Residual impacts of a wildland urban interface fire on urban particulate matter and dust: a study from the Marshall Fire, *Air Qual., Atmos. Health*, 2023, **16**, 1839–1850.
60 D. Calderon-Arrieta, A. C. Morales, A. P. S. Hettiyadura, T. M. Estock, C. Li, Y. Rudich and A. Laskin, Enhanced Light Absorption and Elevated Viscosity of Atmospheric Brown Carbon through Evaporation of Volatile Components, *Environ. Sci. Technol.*, 2024, **58**, 7493–7504.
61 A. L. Hodshire, A. Akherati, M. J. Alvarado, B. Brown-Steiner, S. H. Jathar, J. L. Jimenez, S. M. Kreidenweis, C. R. Lonsdale, T. B. Onasch, A. M. Ortega and J. R. Pierce, Aging Effects on Biomass Burning Aerosol Mass and Composition: A Critical Review of Field and Laboratory Studies, *Environ. Sci. Technol.*, 2019, **53**, 10007–10022.
62 F. K. A. Gregson, N. G. A. Gerrebos, M. Schervish, S. Nikkho, E. G. Schnitzler, C. Schwartz, C. Carlsten, J. P. D. Abbatt, S. Kamal, M. Shiraiwa and A. K. Bertram, Phase Behavior and Viscosity in Biomass Burning Organic Aerosol and Climatic Impacts, *Environ. Sci. Technol.*, 2023, **57**, 14548–14557.
63 A. Moallemi, M. Kazemimanesh, J. C. Corbin, K. Thomson, G. Smallwood, J. S. Olfert and P. Lobo, Characterization of black carbon particles generated by a propane-fueled miniature inverted soot generator, *J. Aerosol Sci.*, 2019, **135**, 46–57.
64 M. Kazemimanesh, A. Moallemi, K. Thomson, G. Smallwood, P. Lobo and J. S. Olfert, A novel miniature inverted-flame burner for the generation of soot nanoparticles, *Aerosol Sci. Technol.*, 2019, **53**, 184–195.
65 H. H. Al-Mashala, M. Schervish, S. M. Liyanage, J. A. Barton, M. Shiraiwa and E. G. Schnitzler, Multiphase Processing of the Water-Soluble and Insoluble Phases of Biomass Burning Organic Aerosol, *ACS ES&T Air*, 2025, **2**, 637–647.
66 H. H. Al-Mashala, K. L. Betz, C. T. Calvert, J. A. Barton, E. E. Bruce and E. G. Schnitzler, Ultraviolet Irradiation Can Increase the Light Absorption and Viscosity of Primary Brown Carbon from Biomass Burning, *ACS Earth Space Chem.*, 2023, **7**, 1882–1889.
67 J. C. Chow, J. Cao, L.-W. Antony Chen, X. Wang, Q. Wang, J. Tian, S. S. H. Ho, A. C. Watts, T. B. Carlson, S. D. Kohl and J. G. Watson, Changes in $PM_{2.5}$ peat combustion source profiles with atmospheric aging in an oxidation flow reactor, *Atmos. Meas. Tech.*, 2019, **12**, 5475–5501.

68 C. D. Cappa, C. Y. Lim, D. H. Hagan, M. Coggon, A. Koss, K. Sekimoto, J. de Gouw, T. B. Onasch, C. Warneke and J. H. Kroll, Biomass-burning-derived particles from a wide variety of fuels – Part 2: effects of photochemical aging on particle optical and chemical properties, *Atmos. Chem. Phys.*, 2020, **20**, 8511–8532.

69 C. F. Fortenberry, M. J. Walker, Y. Zhang, D. Mitroo, W. H. Brune and B. J. Williams, Bulk and molecular-level characterization of laboratory-aged biomass burning organic aerosol from oak leaf and heartwood fuels, *Atmos. Chem. Phys.*, 2018, **18**, 2199–2224.

70 C. Liu-Kang, P. J. Gallimore, T. Liu and J. P. D. Abbatt, Photoreaction of biomass burning brown carbon aerosol particles, *Environ. Sci.: Atmos.*, 2022, **2**, 270–278.

71 M. Mouton, K. A. Malek, M. 'S. H. James, R. P. Pokhrel, M. N. Fiddler, A. A. Asa-Awuku and S. Bililign, The hygroscopic properties of biomass burning aerosol from Eucalyptus and cow dung under different combustion conditions, *Aerosol Sci. Technol.*, 2023, **57**, 665–677.

72 N. G. A. Gerrebos, J. Zaks, F. K. A. Gregson, M. Walton-Raaby, H. Meeres, I. Zigg, W. F. Zandberg and A. K. Bertram, High Viscosity and Two Phases Observed over a Range of Relative Humidities in Biomass Burning Organic Aerosol from Canadian Wildfires, *Environ. Sci. Technol.*, 2024, **58**, 21716–21728.

73 J. Liu, M. Bergin, H. Guo, L. King, N. Kotra, E. Edgerton and R. J. Weber, Size-resolved measurements of brown carbon in water and methanol extracts and estimates of their contribution to ambient fine-particle light absorption, *Atmos. Chem. Phys.*, 2013, **13**, 12389–12404.

74 N. J. Shetty, A. Pandey, S. Baker, W. M. Hao and R. K. Chakrabarty, Measuring light absorption by freshly emitted organic aerosols: optical artifacts in traditional solvent-extraction-based methods, *Atmos. Chem. Phys.*, 2019, **19**, 8817–8830.

75 A. Zhang, Y. Zeng, X. Yang, J. Zhai, Y. Wang, C. Xing, B. Cai, S. Shi, Y. Zhang, Z. Shen, T.-M. Fu, L. Zhu, H. Shen, J. Ye and C. Wang, Organic Matrix Effect on the Molecular Light Absorption of Brown Carbon, *Geophys. Res. Lett.*, 2023, **50**, e2023GL106541.

76 K. L. Raincrow, H. H. Al-Mashala and E. G. Schnitzler, Partitioning of secondary organic aerosol onto nanoplastics leading to hygroscopic partially-engulfed particles, *Environ. Sci.: Atmos.*, 2024, **4**, 9–17.

77 P. E. Dennison, S. C. Brewer, J. D. Arnold and M. A. Moritz, Large wildfire trends in the western United States, 1984–2011, *Geophys. Res. Lett.*, 2014, **41**, 2928–2933.

78 R. F. Hems, E. G. Schnitzler, M. Bastawrous, R. Soong, A. J. Simpson and J. P. D. Abbatt, Aqueous Photoreactions of Wood Smoke Brown Carbon, *ACS Earth Space Chem.*, 2020, **4**, 1149–1160.

79 E. G. Schnitzler, N. G. A. Gerrebos, T. S. Carter, Y. Huang, C. L. Heald, A. K. Bertram and J. P. D. Abbatt, Rate of atmospheric brown carbon whitening governed by environmental conditions, *Proc. Natl. Acad. Sci.*, 2022, **119**, e2205610119.

80 Q. Xie, N. G. A. Gerrebos, D. Calderon-Arrieta, I. S. Morton, E. R. Halpern, C. Li, M. F. Zeng, A. K. Bertram, Y. Rudich and A. Laskin, Molecular Insights into Gas–Particle Partitioning and Viscosity of Atmospheric Brown Carbon, *Environ. Sci. Technol.*, 2024, **58**, 18284–18294.

81 A. L. Hodshire, E. Ramnarine, A. Akherati, M. L. Alvarado, D. K. Farmer, S. H. Jathar, S. M. Kreidenweis, C. R. Lonsdale, T. B. Onasch, S. R. Springston, J. Wang, Y. Wang, L. I. Kleinman, A. J. Sedlacek III and J. R. Pierce, Dilution impacts on smoke aging: evidence in Biomass Burning Observation Project (BBOP) data, *Atmos. Chem. Phys.*, 2021, **21**, 6839–6855.

82 M. L. Roson, M. Abou-Ghanem, E. Kim, S. Wu, D. Long, S. A. Styler and R. Zhao, Unexpected electrophiles in the atmosphere – anhydride nucleophile reactions and uptake to biomass burning emissions, *Phys. Chem. Chem. Phys.*, 2023, **25**, 18742–18756.

83 R. Saleh, C. J. Hennigan, G. R. McMeeking, W. K. Chuang, E. S. Robinson, H. Coe, N. M. Donahue and A. L. Robinson, Absorptivity of brown carbon in fresh and photo-chemically aged biomass-burning emissions, *Atmos. Chem. Phys.*, 2013, **13**, 7683–7693.

84 P. Beeler, J. Kumar, J. P. Schwarz, K. Adachi, L. Fierce, A. E. Perring, J. M. Katich and R. K. Chakrabarty, Light absorption enhancement of black carbon in a pyrocumulonimbus cloud, *Nat. Commun.*, 2024, **15**, 6243.

85 M. Gysel, G. B. McFiggans and H. Coe, Inversion of tandem differential mobility analyser (TDMA) measurements, *J. Aerosol Sci.*, 2009, **40**, 134–151.

86 M. R. Stolzenburg and P. H. McMurry, Equations Governing Single and Tandem DMA Configurations and a New Lognormal Approximation to the Transfer Function, *Aerosol Sci. Technol.*, 2008, **42**, 421–432.

87 N. G. A. Gerrebos, J. Zaks, F. K. A. Gregson, M. Walton-Raaby, H. Meeres, I. Zigg, W. F. Zandberg and A. K. Bertram, High Viscosity and Two Phases Observed over a Range of Relative Humidities in Biomass Burning Organic Aerosol from Canadian Wildfires, *Environ. Sci. Technol.*, 2024, **58**, 21716–21728.

88 M. Bilde, K. Barsanti, M. Booth, C. D. Cappa, N. M. Donahue, E. U. Emanuelsson, G. McFiggans, U. K. Krieger, C. Marcolli, D. Topping, P. Ziemann, M. Barley, S. Clegg, B. Dennis-Smither, M. Hallquist, Å. M. Hallquist, A. Khlystov, M. Kulmala, D. Mogensen, C. J. Percival, F. Pope, J. P. Reid, M. A. V. Ribeiro da Silva, T. Rosenoern, K. Salo, V. P. Soonsin, T. Yli-Juuti, N. L. Prisle, J. Pagels, J. Rarey, A. A. Zardini and I. Riipinen, Saturation Vapor Pressures and Transition Enthalpies of Low-Volatility Organic Molecules of Atmospheric Relevance: From Dicarboxylic Acids to Complex Mixtures, *Chem. Rev.*, 2015, **115**, 4115–4156.

89 C. Mosselman, W. H. Van Vugt and H. Vos, Exactly integrated Clapeyron equation. Its use to calculate quantities of phase change and to design vapor pressure-temperature relations, *J. Chem. Eng. Data*, 1982, **27**, 246–251.

90 V. M. Donovan, R. Crandall, J. Fill and C. L. Wonkka, Increasing Large Wildfire in the Eastern United States, *Geophys. Res. Lett.*, 2023, **50**, e2023GL107051.

